NINTH EUROPEAN ROTORCRAFT FORUM

Paper No. 50

A GENERAL MODEL OF HELICOPTER BLADE DYNAMICS

A. ROSEN and O. RAND

Department of Aeronautical Engineering
Technion - Israel Institute of Technology
Haifa, Israel

September 13-15, 1983

STRESA, ITALY

Associazione Industrie Aerospaziali

Associazione Italiana di Aeronautica ed Astronautica

A General Model of Helicopter Blade Dynamics

A. Rosen and O. Rand

Department of Aeronautical Engineering
Technion - Israel Institute of Technology
Haifa, Israel

Abstract

A general model which describes the helicopter blade dynamics is presented. The hub center may have any combination of linear or angular velocities and accelerations. In addition, the blade root can move relative to the shaft and this motion is general and does not include the assumption of small angles or small displacements. The root dynamics may be considered as an input to the model or is determined by applying equilibrium considerations. The structural model of the blade itself is that of a curved slender rod. Nonlinear effects are included in this structural model. The treatment of the inertia loads is also a very general one and includes all the nonlinear contributions due to the blade motions and deflections. The present paper concentrates on the modeling of the blade motions, structural behavior and inertia loads and therefore a relatively simple aerodynamics is used, but as a result of the flexibility of the complete model and its modular construction, any description of the aerodynamic loads can be adopted quite easily. Integration with respect to time of the complete system of equations of motion, yields the root motions and blade elastic deformations. In order to present the flexibility and capabilities of the model, a few numerical examples are presented. The results are discussed and important conclusions are pointed out.

1. Introduction

During the years and as a result of the increasing computational capabilities, general models of helicopter blade dynamics have been developed. Descriptions of such models and the associated computer codes appear in [1-6] (these are representative examples while other similar models have also been described in the literature). Although such models are very general they always include different assumptions which restrict their use and cause increasing errors in certain cases. The purpose of the present paper is to present a new general model of the blade dynamics where an effort has been done to avoid unnecessary assumptions and to obtain a tool which is capable of dealing with cases which cannot be treated with other existing models.

Some of the special features of the model are:

a) The analysis is not restricted to straight blades and includes the case of planar curved blades.

b) The structural model of the blade includes nonlinear effects. At the

moment the structural analysis is restricted to the case of small strains and moderate rotation, but if necessary, the structural model can be extended quite easily to include cases of higher nonlinearities.

c) The inertia loads are accurate and the nonlinear influences of the deformations on these loads are included.

d) A special model of the root dynamics enables the modelling of almost any kind of hub and any kind of attachment of the blade to the hub. This includes elastomeric bearings and any other flexible kinds of attachments.

e) The resultant moment and resultant shearing forces along the blade are calculated by integration and include all the nonlinear effects. In addition, the resultant moments can also be obtained by differentiation of the displacements.

The above mentioned features and others are explained in what follows. The present model is in fact the application of a recently developed [7] general model of the dynamics of moving and rotating curved rods, to the analysis of helicopter blades. The detailed equations and derivations are presented in [7]. Here only the details which are necessary in order to understand the model, are brought. The paper will concentrate on presenting the generality, accuracy and flexibility of the model.

2. General Description of the Model

2.1 The Systems of Coordinates

The basic system of coordinates is the F system which is shown in Fig. 1. The origin of this system is placed at the hub center while z_F

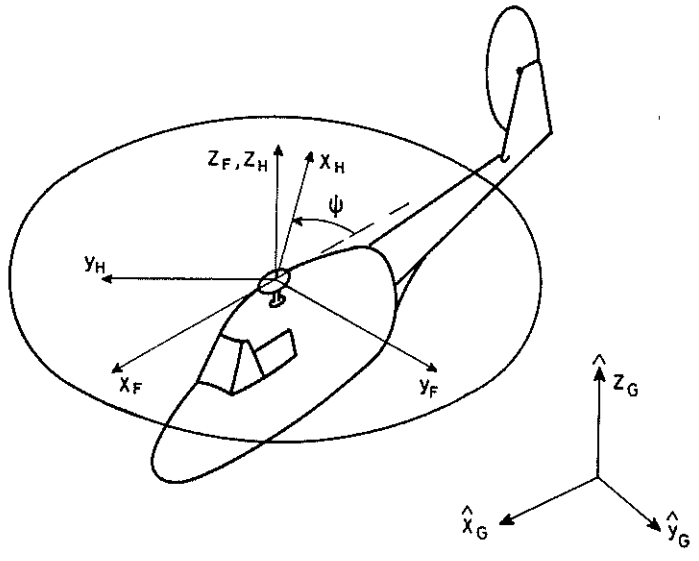

Fig. 1. The G, F and H systems of coordinates.

coincides with the shaft direction and x_F points towards the helicopter front. This is a cartesian system which does not rotate with the hub. $\hat{x}_F$, $\hat{y}_F$ and $\hat{z}_F$ are unit vectors in the direction of the coordinates lines x_F, y_F and z_F, respectively. The F system moves due to the fuselage motions and motions of the shaft (not including the rotation) relative to the fuselage. The dynamics of the origin of the F system is described by: a linear velocity $\bar{V}_{FG}$, a linear acceleration $\bar{a}_{FG}$, an angular velocity $\bar{Q}_{FG}$ and an angular acceleration $\dot{\bar{Q}}_{FG}$. All the velocities and accelerations are measured relative to the G system (see Fig. 1) which is an inertial system of coordinates, fixed with respect to the earth. $\hat{x}_G$, $\hat{y}_G$ and $\hat{z}_G$ are unit vectors in the directions of the coordinate lines of the G system while the gravity acceleration, g, acts in the $\hat{z}_G$ direction. The transformation between the F system and G system at any moment is known and is a function of the fuselage motion and the shaft inclination relative to the fuselage.

The velocities and accelerations of the F system are described as follows:

$$\bar{V}_{FG} = V_{xF}\hat{x}_F + V_{yF}\hat{y}_F + V_{zF}\hat{z}_F \tag{1-a}$$

$$\bar{a}_{FG} = a_{xF}\hat{x}_F + a_{yF}\hat{y}_F + a_{zF}\hat{z}_F \tag{1-b}$$

$$\bar{Q}_{FG} = p\hat{x}_F + q\hat{y}_F + r\hat{z}_F \tag{1-c}$$

$$\dot{\bar{Q}}_{FG} = S_{xF}\hat{x}_F + S_{yF}\hat{y}_F + S_{zF}\hat{z}_F \tag{1-d}$$

The third system of coordinates is the H (hub) system, which is rotating with the hub (see Fig. 1). The coordinate lines of this system are x_H, y_H and z_H while $\hat{x}_H$, $\hat{y}_H$ and $\hat{z}_H$ are unit vectors in these directions, respectively. The coordinate lines z_F and z_H coincide, while the H system is rotated about the z_F axis in an angular velocity Ω, relative to the F system. In general Ω is a function of time. As shown by Fig. 1, ψ is the azimuth angle of the H system relative to the F system (ψ is measured relative to the negative direction of x_F). When $\psi = \pi$ the two systems (F and H) coincide.

The next system of coordinates is the blade system which is denoted the B system. The coordinate lines of this system are x_B, y_B and z_B while $\hat{x}_B$, $\hat{y}_B$ and $\hat{z}_B$ are unit vectors in these direction, respectively.

The transformation from the H system to the B system is described in Fig. 2 and is composed of linear displacements f_x, f_y, f_z in the directions x_F, y_F, z_F, respectively and rotations β (flapping), ζ (lead lag), θ (pitch) (see Fig. 2). f_x, f_y, f_z, β, ζ and θ are in general functions of time and there are no restrictions on their magnitude. Since β, ζ and θ are finite angles, their sequence is important in determining the

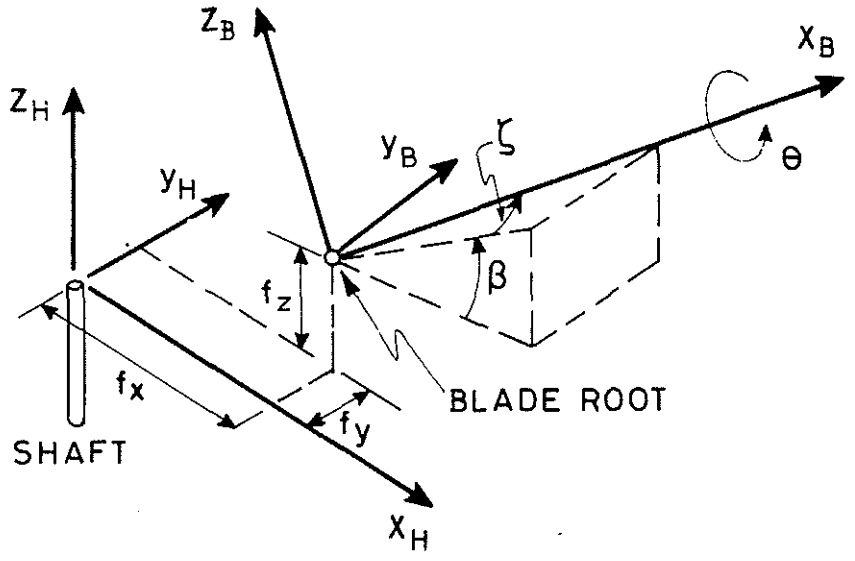

Fig. 2. The root motions.

transformation between the H and B systems. In Fig. 2 the case where the flapping hinge is the inner one and the pitch bearing is the outer one, is presented. Any other sequence of the rotation angles can be treated. In such case one has only to recalculate the terms of the transformation matrix which are functions of these three angles, and the time derivatives of the transformation matrix (for details see [7]).

The B system of coordinates is used in order to describe the elastic axis of blade (see Fig. 3). The present derivation is restricted to the case of a planar curved blade where the elastic axis lies in the plane which is defined by the coordinate lines x_B and y_B. x is a curved coordinate line along the elastic axis of the blade which is equal to zero at the blade root and is equal to L at the blade tip. L is the length of the blade. As shown in Figs. 2, 3, the blade root is positioned at the origin of coordinates of the B system. The shape of the undeformed elastic axis is described by $x_B(x)$ and $y_B(x)$. At each point along the blade an orthogonal triad of unit vectors $\hat{e}_x$, $\hat{e}_y$ and $\hat{e}_z$ is defined. $\hat{e}_x$ is tangent to the elastic axis at each point while $\hat{e}_y$ is perpendicular to $\hat{e}_x$ and lies in the plane which is defined by the coordinate lines x_B and y_B, $\hat{e}_z$ is perpendicular to this plane (see Fig. 3). The local sweep angle of the blade (the angle between $\hat{e}_x$ and $\hat{x}_B$) is denoted η.

The blade deforms as a result of the loads which are distributed along it. This deformation is described by the displacement of each point along the elastic axis. The components of this displacement are u, v, w in the directions $\hat{e}_x$, $\hat{e}_y$ and $\hat{e}_z$, respectively (see Fig. 3). In addition, each cross section is also rotated by an angle ϕ about the elastic axis. Due to this deformation, the triad $\hat{e}_x$, $\hat{e}_y$, $\hat{e}_z$, at a certain point of the undeformed axis, is transformed into a new rotated orthogonal triad of unit

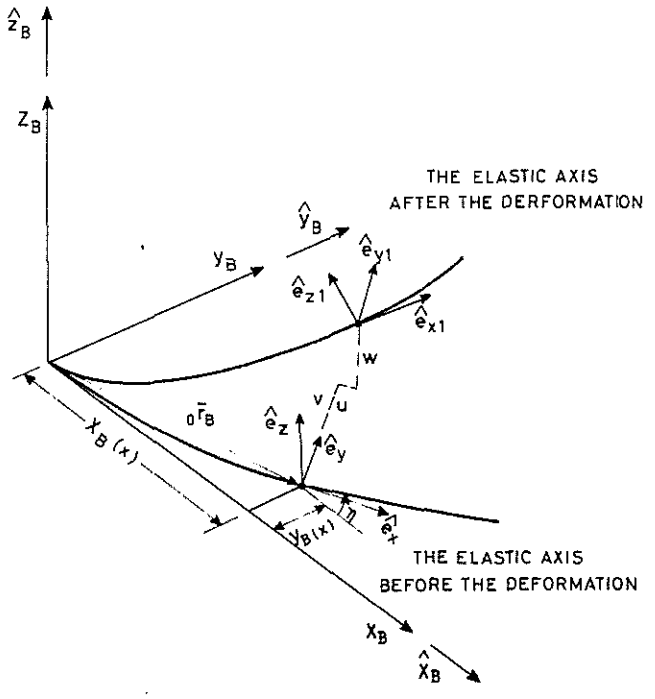

Fig. 3. The elastic axis before and after the deformation.

vectors $\hat{e}_{x1}$, $\hat{e}_{y1}$ and $\hat{e}_{z1}$, respectively (see Fig. 3). The rotation of the triad e_x, e_y, e_z to the new triad e_{x1}, e_{y1}, e_{z1}, is not restricted to small angles and is therefore described by Euler angles. In [7] the general exact expression for the transformation matrix between the two triads of unit vectors, as function of u, v, w, ϕ, is given. From the exact expression the transformations for different stages of approximations are obtained. The first approximation is that of small extensions of the elastic axis (the relative extension is small compared to unity). This assumption is applicable, to all the practical cases of blades which are manufactured from regular engineering materials, that undergo only small strains. The second stage of assumptions is that of small strains and moderate rotations. The most severe assumption, which yields the simplest transformation matrix, is that of small strains and small rotations.

2.2 The Structural Model of the Blade

The detailed derivation of the structural model is presented in [7]. Here, only the details which are essential in order to understand the model and the assumptions behind it, are discussed.

From a structural point of view the blade is considered as a curved slender rod. The basic assumption which is adopted here is the well known Bernoulli-Euler hypothesis. This hypothesis has been proved to give very good results in the case of slender rods. This hypothesis states that:

a) Plane cross sections which are normal to the elastic axis before the deformation remain plane after the deformation (except for very small deviations due to warping) and normal to the deformed elastic axis.

b) Strains within the cross section can be neglected.

Based on this hypothesis, it is possible now to describe the deformation of each point of the blade (points that are not on the elastic axis) by the deformations of the elastic axis. Each material point of the blade before the deformation is defined by the three coordinates x, y, z. As already indicated before, x is a curvilinear coordinate along the undeformed elastic axis and it defines the cross section of the blade where the material point is located. y and z are cross sectional coordinates (in the $\hat{e}_y$ and $\hat{e}_z$ directions, respectively) which determine the cross sectional location of the point. The position vector of any material point (x, y, z) after the deformation, relative to the origin of the B system, is given by (see Fig. 3):

$$\bar{R}_B(x,y,z) = x_B\hat{x}_B + y_B\hat{z}_B + u\hat{e}_x + v\hat{e}_y + w\hat{e}_z + y\hat{e}_{y1} + z\hat{e}_{z1} + T(x)\phi(x,y,z)\hat{e}_{x1} \quad (2)$$

ϕ is the St. Venant warping function of the cross section while T is the elastic twist. Therefore, $T\phi$ is the warping displacement which can be considered as an extension of the classical St. Venant torsion. The derivation is restricted to the practical cases of small warping displacements where the displacements are negligible compared to typical cross sectional dimensions of the blade.

After the position vectors before and after deformation, of each point of the blade, have been defined, it is possible to calculate the strain components along the blade using well known definitions of solid mechanics. Afterwards, the stress components are obtained from the strain components by using the stress-strain relations for the case of slender rods. Integration of stresses over the blade's cross section implies the cross sectional resultant force $\bar{F}$ and resultant moment $\bar{M}$, which are described by their components as follows:

$$\bar{F} = P\hat{e}_{x1} + V_y\hat{e}_{y1} + V_z\hat{e}_{z1} \quad (3)$$

$$\bar{M} = M_x\hat{e}_{x1} + M_y\hat{e}_{y1} + M_z\hat{e}_{z1} \quad (4)$$

The expressions for P, M_x, M_y and M_z include the cross sectional uctural properties, and the elastic twist and curvatures. The elastic st and curvatures are fractions of the initial curvature of the blade, and the displacement components and their derivatives with respect to more details see [7]).

The blade is acted upon by a distributed force $\bar{p}$ and a distributed

moment $\bar{q}$, per unit length. These loads include aerodynamic and inertia contributions. $\bar{p}$ and $\bar{q}$ are described by their components as follows:

$$\bar{p} = p_x \hat{e}_{x1} + p_y \hat{e}_{y1} + p_z \hat{e}_{z1} \tag{5}$$

$$\bar{q} = q_x \hat{e}_{x1} + q_y \hat{e}_{y1} + q_z \hat{e}_{z1} \tag{6}$$

If equilibrium of forces and moments on a small segment of the blade is considered, four equations in the four unknowns: v, w, ϕ and P - are obtained. v, w and P are nondimensional terms which are defined by the following relations:

$$\overset{\circ}{v} = v/L \ , \ \overset{\circ}{w} = w/L \ , \ \overset{\circ}{P} = PL^2/Eb^4 \tag{7}$$

E is a representative Young's Modulus of the blade material while b is a typical cross sectional dimension. the nondimensional axial component of the resultant force ($\overset{\circ}{P}$) is replacing u as an unknown. This replacement is very common in blade analysis and it has a few advantages which will not be discussed here. As a result of this replacement the axial component of the displacement at each moment (u), becomes a function of the four unknowns. The four equilibrium equations are nonlinear while the present derivation is restricted to the case of small strains and moderate elastic rotations.

The equilibrium equations are solved by using Galerkin method. According to this method the unknowns are described by the following series:

$$\overset{\circ}{v} = \sum_{j=1}^{N_v} v_j \, FV_j \tag{8-a}$$

$$\overset{\circ}{w} = \sum_{k=1}^{N_w} w_k \, FW_k \tag{8-b}$$

$$\phi = \sum_{l=1}^{N_\phi} \phi_l \, F\phi_l \tag{8-c}$$

$$\overset{\circ}{P} = \sum_{m=1}^{N_p} p_m \, FP_m \tag{8-d}$$

FV_j, FW_k, $F\phi_l$ and FP_m are functions of x which are defined in the region $0<x<L$. The series should satisfy the boundary condition at the blade edges. At the tip the conditions are those of a free edge, namely: the resultant force and moment are equal to zero. The conditions at the blade root depend on the nature of this root which is a function of the method by which the blade is attached to the hub and the control elements. More about these conditions appear in subsection 2.5.

The coefficients v_j, W_k, ϕ_l and p_m are in general functions of time. The numbers of terms in the series (N_v, N_w, N_ϕ and N_p) have a significant influence on the accuracy of the solution. In the present code there is not any restriction on the total number of terms, but a large number means a significant increase in the required computer memory and time of computations. The total number of unknowns, N, equals:

$$N = N_v + N_w + N_\phi + N_p \tag{9}$$

The equations of equilibrium are divided into two groups. The first group is the equations which mainly describe the axial equilibrium of forces. These equations are:

$$[A_2]\{S_p\} = -[A_1]\{S_r\} + \{d_p\} \tag{10}$$

$[A_1]$ is an $N_p x(N-N_p)$ matrix while $[A_2]$ is an $N_p x N_p$ square matrix. These matrices present structural properties of the blade. $\{S_p\}$ and $\{S_r\}$ are vectors of unknowns defined as:

$$\{S_p\}^T = \langle p_1, \ldots, p_m, \ldots, p_{N_p} \rangle \tag{11}$$

$$\{S_r\}^T = \langle v_1,\ldots,v_j,\ldots,v_{N_v},w_1,\ldots,W_k,\ldots,W_{N_w}, \phi_1,\ldots,\phi_l,\ldots\phi_{N_\phi} \rangle \tag{12}$$

The load vector $\{d_p\}$ is given by:

$$\{d_p\}^T = \langle HP5_{(1)},\ldots,HP5_{(mn)},\ldots,HP5_{(N_p)} \rangle \tag{13}$$

where:

$$HP5_{(mn)} = \frac{1}{L}\int_0^L P_x \, FP_{mn} \, dx \tag{14}$$

P_x is a generalized force defined as:

$$P_x = \frac{L^3}{Eb^4}(-p_{xe}-\chi_y q_{ze}) \tag{15}$$

p_{xe} and q_{ze} are equivalent components which differ from p_x and q_z by the fact that they also include nonlinear structural contributions. The nonlinear structural contributions in this case are looked upon as "additional quasi loads" (for more details see [7]).

The second group of equations is described by the following matrix notation:

$$[A_3]\{S\} = \{d_s\} \tag{16}$$

$[A_3]$ is an $(N-N_p)xN$ matrix which presents structural properties. $\{S\}$ is the complete vector of unknowns which is defined as:

$$\{S\} = \begin{Bmatrix}\{S_r\}\\ \{S_p\}\end{Bmatrix} \tag{17}$$

$\{d_s\}$ is the loading vector, which is given by:

$$\{d_s\} = \langle HV6_{(1)},\ldots,HV6_{(jn)},\ldots,HV6_{(N_v)},HW6_{(1)},\ldots,HW6_{(kn)},$$

$$\ldots,HW6_{(N_w)},H\phi4_{(1)},\ldots,H\phi4_{(ln)},\ldots,H\phi4_{(N_\phi)}\rangle \tag{18}$$

where:

$$HV6_{(jn)} = \frac{1}{L}\int_0^L P_y\, FV_{jn}\, dx \tag{19-a}$$

$$HW6_{(kn)} = \frac{1}{L}\int_0^L P_z\, FW_{kn}\, dx \tag{19-b}$$

$$H\phi4_{(ln)} = \frac{1}{L}\int_0^L P_\phi\, F\phi_{ln}\, dx \tag{19-c}$$

The generalized forces P_y, P_z, P_ϕ are defined below:

$$P_y = \frac{L^3}{Eb^4}\left(-p_{ye}+\partial q_{ze}/\partial x\right) \tag{20-a}$$

$$P_z = \frac{L^3}{Eb^4}\left(-p_{ze}-\partial q_{ye}/\partial x\right) \tag{20-b}$$

$$P_\phi = -\, q_{xe}L^2/Eb^4 \tag{20-c}$$

The equilibrium equations and their derivation have been described only briefly. Detailed description can be found in [7].

As indicated before, expressions for the cross sectional resultant

forces and moments are obtained during the course of the derivation. These expressions include high derivatives of the displacements. It is well known from numerical analysis that differentiation of the approximate expression for the displacements yields increasing errors, as the order of the derivation is increased. Therefore it is expected that while the accuracy of the approximate solutions of the displacements may be satisfactory, the resultant moment and force components, which are obtained by differentiation, will exhibit increasing errors.

In order to obtain better results, another method of calculating the resultant force and moment has been adopted. According to this method these resultants are obtained by integration of the loads from the blade tip to a specific cross section where the resultant force and moment are calculated. In these calculations the influences of the deformation are taken into account in an exact manner. In [7] detailed description of the integration procedure is given. In the numerical results which will be presented in this paper, comparisons between the results of both methods (differentiation and integration) will be presented.

2.3 The Inertia Loads

In order to calculate the inertia loads it is necessary at first to calculate $\bar{a}_G$ which is the acceleration of each point of the blade relative to the G (inertial) system. In [7], the detailed derivation of $\bar{a}_G$ is presented. At first it is assumed that the position vector of each point of the blade, relative to the origin of the B system or coordinates, is given by Eq. (2). Since the derivation is restricted to the practical cases where the warping displacements are very small, the warping displacements and their time derivatives are neglected in the acceleration calculations. Except from this assumption the derivation is exact and it is not assumed that any of the variables or its derivatives are small and negligible compared to other terms. Unlike the structural model, the transformation matrix between $\hat{e}_x$, e_y, e_z and e_{x1}, e_{y1}, e_{z1} is exact and the assumption of moderate relations is not used. Because of this accuracy the derivation is very complicated and therefore matrix notation is used throughout the whole derivation. It should be emphasized that $\bar{a}_G$ is a function of f_x, f_y, f_z, ϕ, ζ, β and their time derivates. It is clear that it is also a function of $\bar{V}$, $\bar{a}_{FG}$, $\bar{\Omega}_{FG}$ and $\dot{\bar{\Omega}}_{FG}$ which are given by Eqs. (1-a-d).

According to D'Alembert's principle, the inertia force $\bar{f}_I$ which acts on each element of mass of the blade, equals:

$$\bar{f}_I = - \rho \bar{a}_G dydzdx \qquad (21)$$

Therefore the distributed inertia force per unit length of the blade becomes:

$$\bar{p}_I = -\int_A \int \rho \bar{a}_G dydz \tag{22}$$

The distributed moment about the elastic axis, due to inertia loads, is given by:

$$\bar{q}_I = \int_A \int (y\hat{e}_{y1} + z\hat{e}_{z1}) x \bar{f}_I dydz \tag{23}$$

2.4 The Equations of Motion

By substitution of the inertia loads into the equilibrium equations and after a few mathematical operations, the equations of motion are obtained:

$$\{S_p\} = [A_2]^{-1}\{-[A_1]\{S_r\} + \{d_p\}\} \tag{24-a}$$

$$\{\ddot{S}_r\} = [D]^{-1}\{[A_3]\{S\} - \{d_r\}\} \tag{24-b}$$

an upper dot indicates a differentiation with respect to time. Equation (24-a) is obtained directly from Eq. (10). $\{d_r\}$ in Eq. (24-b) differs from $\{d_s\}$ of Eq. (16) by the fact that part of the inertia loads ($[D]\{\ddot{S}_r\}$) have been separated from the other loads and they have yielded the terms on the left side of the equation. $[D]$ is a $[(N-N_p)x(N-N_p)]$ matrix which presents the inertia (mass) properties of the blade. $[A_2]^{-1}$ and $[D]^{-1}$ are calculated only once at the beginning of the solution procedure and stored. At the beginning of each time step $\{S_p\}$ is calculated first by solving Eq. (24-a) and then the accelerations are calculated by using Eq. (24-b). Now an integration step is carried out and the procedure is repeated again.

From Eqs. (24-a,b) it is clear that the pure axial dynamics, which include axial vibrations along the blade (waves), are not dealt with in the present analysis. These dynamics are not important in analysing blade behavior. On the other hand it should be clear that the inertia loads include the influences of $\dot{u}$ and $\ddot{u}$ which are calculated at each moment, as has been described previously.

2.5 The Root Dynamics

As indicated before, the right side of Eqs. (24-a,b) includes expressions of f_x, f_y, f_z, β, ζ, θ and their first and second time derivatives. There are cases where these variables (or part of them), as functions of time, are known a priori. Such cases include hingeless rotors where f_x, f_y, f_z, β and ζ are known constants, or blades where the pitch angle is considered as a known command input (rotors whre the flexibility of the control system is neglected). The other cases are those where few of the variables are determined from equilibrium considerations at the blade root. Such a case is, for example, the conventional articulated rotor where β and ζ are determined at each moment from the condition of equilibrium of moments at the blade root.

In general, the root dynamics is described by the following equation:

$$\{\ddot{q}_r\} = \{Q\} \tag{25}$$

where

$$\{q_r\}^T = \langle f_x, f_y, f_z, \beta, \zeta, \theta \rangle \tag{26}$$

$\{Q\}$ in general is a complicated nonlinear function of $\{q_r\}$, $\{S_r\}$, $\{S_p\}$ and their time derivatives.

This general representation of the root dynamics enables one to model accurately any kind of rotor, like: hingeless, articulated, gimballed, teetering and others. In each case the vector $\{Q\}$ is derived and implemented into the computer code.

As an example, the case of a blade which is free to rotate about the flapping hinge is considered. f_x, f_y, f_z and ζ are kept constant while θ is a known function of time. As explained previously, the resultant moment along the blade can be calculated at any time. The resultant moment at the blade root is described as follows:

$$\bar{M}(0) = M_{xB}(0)\hat{x}_B + M_{yB}(0)\hat{y}_B + M_{zB}(0)\hat{z}_B \tag{27}$$

The moment about the flapping hinge will therefore be (see Fig. 2):

$$M_{\beta B} = M_{xB}(0)\ \sin\zeta - M_{yB}(0)\ \cos\zeta\cos\theta + M_{zB}(0)\ \cos\zeta\sin\theta \tag{28}$$

The flapping equation of motion becomes:

$$I\ddot{\beta} = \tilde{M}_{\beta B} \tag{29}$$

I is the blade moment of inertia about the flapping hinge. $\tilde{M}_{\beta B}$ is similar to $M_{\beta B}$ and the only difference between both is the fact that $\tilde{M}_{\beta B}$ does not include the influence of linear terms in $\ddot{\beta}$. (It is clear that these terms are included in $M_{\beta B}$ since they represent important contributions of the inertia loads). They are neglected in $\tilde{M}_{\beta B}$ since their influence already appears in the term on the left side of Eq. (29). More details about this problem and the method of dealing with it appear in [7].

It is worth pointing out again that it has not been assumed that β, or θ are small angles, and they can obtain any finite value.

The example which has been presented here is a relatively simple one. In a similar manner more complicated cases can be dealt with. Any spring at the blade root, linear or nonlinear, and any damping like those which can

result from elastomeric bearings can be modeled by adding appropriate root moments while assembling the vector{Q}. Example of such case appear in the next section.

2.6 Integration of the Equations of Motion

In order to find the behavior of the blade, integration of Eqs. (24-a,b) and (25) is carried out. In the present analysis an implicit Adam's method [8] is used for the integration, while the relative error is not exceeding 0.001. It has been found that this method is relatively efficient and yields very good results. On the other hand it should be noted that because of the modular construction of the computer code it is possible to replace this integration scheme by any other scheme without any alterations of the other parts of the code. During the integration, at certain azimuthal locations which are specified by the operator of the code, the distributions of the deformations and loads along the blade are printed as tables or plotted. Examples of these will be presented in what follows.

3. Numerical Results

The purpose of this section is to present the capabilities and flexibility of the present model and associated computer code. There are a few examples which are outlined below. In all the cases straight blades are considered while cases of curved blades will be reported in the future.

The aerodynamic model which will be used in all the examples is relatively simple.

Aerodynamic description of the blade cross section is presented in Fig. 4. U_p and U_T are the components of the velocities at the blade cross

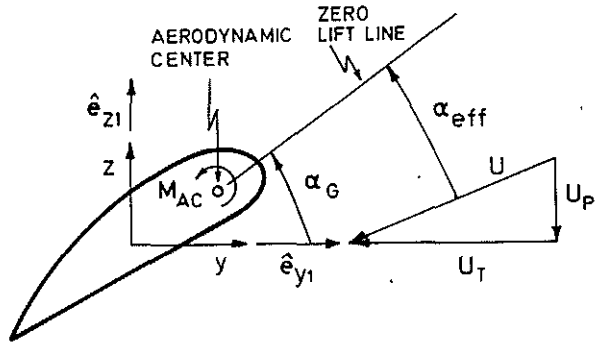

Fig. 4. Cross sectional aerodynamic description.

section which includes the influences of the rotor motions, root motions, elastic deformations and the induced velocity. The relatively simple blade element theory is used here in order to calculate the aerodynamic lift and drag. The lift coefficient is obtained by multiplying the lift coefficient curve slope by the effective angle of attack, α_{eff}. Nonlinear aerodynamic

phenomena are not taken into account. The drag coefficient C_D is given by:

$$C_D = \delta_0 + \delta_1 \alpha_{eff} + \delta_2 \alpha_{eff}^2 \qquad (30)$$

In all the cases which will be considered here the aerodynamic center will coincide with the elastic center. Therefore, since in all the cases the aerodynamic moment coefficient is equal to zero, the only aerodynamic moment is the well known pitch damping [9], which (in the present case) is approximately given by:

$$q_{xa} \tilde{=} - \pi \rho_A C^3 U \dot{\phi}/8 \qquad (31)$$

c is the chord, ρ_A the air density and U the resultant velocity. Tip losses are not taken into account in the present analysis.

3.1 Flapping Hinge - Solution Without Root Dynamics

The properties of the blade are given in the Appendix. This is a uniform blade where the structural, mass and aerodynamic properties are constant along it. There is not any spanwise aerodynamic, mass or structural twist. It can be seen that the blade is relatively stiff. Therefore nonlinear structural effects have minor importance since (as it will be shown later in this section) the elastic deformations are relatively small compared to the rigid body displacement. On the other hand it should be noted that the transformation matrices and their time derivatives are accurate and include all the nonlinar terms which seem to have nonnegligible influence on certain variables. As indicated in the Appendix, there is not a primary structural coupling between the flapping and lead-lag deformations ((EI_{yz}) is equal to zero). On the other hand there is a compound component of the cross sectional mass moment of inertia (MI_{yz}) which has a significant influence on the torsional behavior of the blade.

The conditions at the blade root are such that f_x, f_y and f_z are constant and equal to zero. The blade is free to rotate about the flapping hinge but is clamped with respect to the lead-lag motions (ζ=0), and the angle θ is also kept equal to zero. While θ is equal to zero there is on the other hand a constant aerodynamic pitch angle α_G (see Fig. 4) along the blade which is equal to eight degrees.

As already mentioned in the beginning of the section, the aerodynamic model is very simple. On the other hand, since the main purpose of this paper is to present the dynamic model of the blade, a relatively extreme dynamic case is treated here. The severity of the case is indicated by the very high accelerations which appear during the blade response. It is assumed that the motion of one of the blades of a hovering rotor has been suddenly disturbed and when this blade is at azimuthal location ψ=0 the flapping angle and the flapping velocity are equal to zero. In addition, all the elastic displacements are also equal to zero at this moment (ψ=0). The purpose now is to find the blade response. In order to concentrate on the dynamic behavior and to simplify the aerodynamic analysis, it is assumed that during the whole dynamic response the inflow is equal to the inflow at the

steady state which is equal to 0.04 (This is the uniform induced velocity divided by the tip velocity.)

Two terms are used in the series which describes $\dot{v}$ ($N_v = 2$, see Eq. 8-a). Since the blade is clamped at the root with respect to the lead-lag motions, FV_j are chosen as the first and second normalized modes of a uniform clamped free beam [10]. The series which describes $\dot{w}$ includes three terms. The first term describes the rigid body flapping and is simply x/L. The two other terms (FW_2, FW_3) are the first and second normalized elastic modes of vibration of a simply-supported/free beam [10]. $F\phi_1$ and $F\phi_2$ are the first and second torsional modes of a fixed/free uniform circular beam. The series for $\dot{P}$ includes the following terms:

$$FP_1 = 1 - (x/L)^2$$

$$FP_m = \sin[\pi(m-1.5)(1-x/L)] \qquad m \geq 2 \tag{32}$$

As one should recall, at any moment, $\dot{P}$ is obtained directly from the other unknowns and is not itself one of the unknowns which are integrated with respect to time. Therefore five terms ($N_p = 5$) are included in the series which describes $\dot{P}$, without causing a significant increase in the magnitude of the problem.

In Fig. 5 the different coefficients, as functions of the azimuthal location of the blade (nondimensional time), are presented. The most interesting coefficients are those which describe the flapping motions (w_1, w_2, w_3). w_1, as indicated before, presents the highly damped rigid body flapping. This rigid body flapping can also be calculated analytically by applying different assumptions which imply a second order ordinary differential equation of the flapping, that can be solved quite easily (see for example [11] section 2.6). The agreement between the analytical results and w_1 has been checked and it was so good that both curves practically coincided. As can be seen w_2 is much smaller than w_1 while w_3 is much smaller than w_2 and therefore it can concluded that the convergence is very good. w_2 approaches a steady state while it vibrates in its natural frequency which is approximately 7/rev. w_3 exhibits a respons which is the combination of the frequency of w_2 and its own frequency which is approximately three times higher.

In general, the lead-lag motions ($\dot{v}$) are almost three orders of magnitude smaller than the flapwise motions. The behavior of v_1 is composed of an initial response (from ψ=0 up to ψ=130°) which is followed by lightly damped vibrations. It is interesting to note that the frequency of v_1 coincides with the frequency of w_2. Since both, the vibrations of v_1 and w_2, are in phase it seems that they influence one another. v_2 is much smaller than v_1 and its response is composed of low frequency vibrations above which the high frequency natural vibrations of v_2 are superimposed.

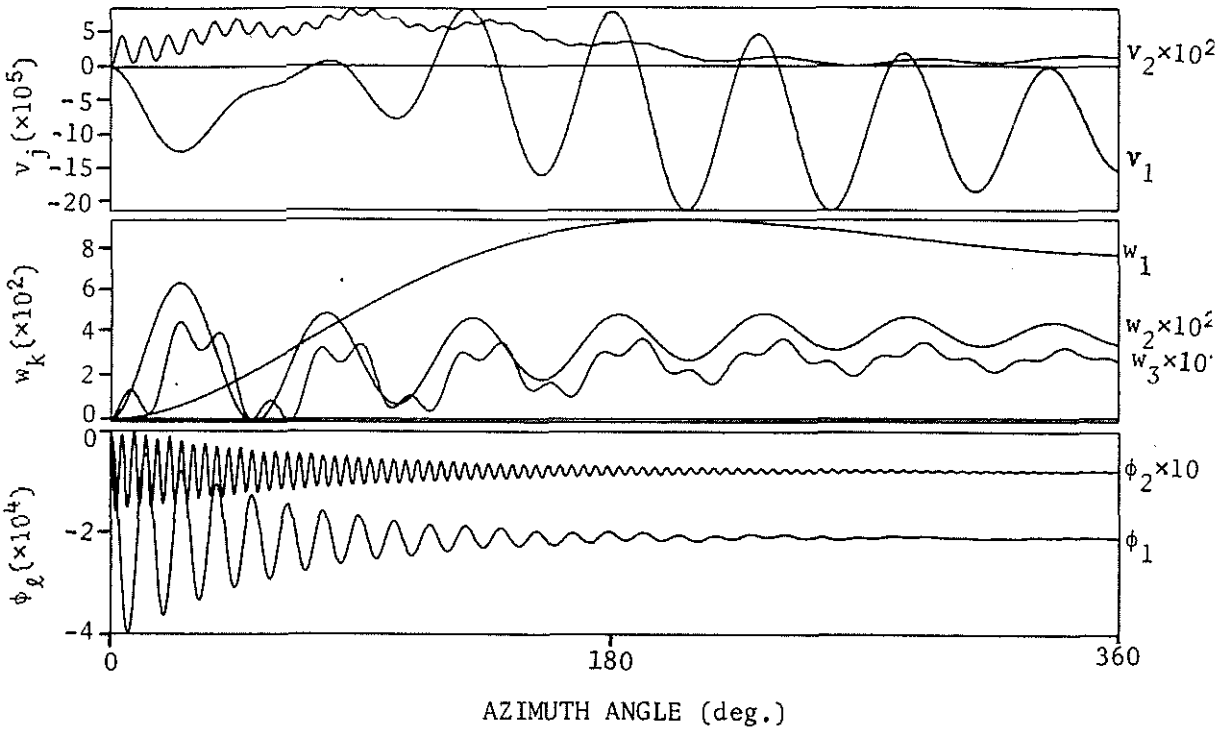

Fig. 5. Case 3.1 - Time Response of the Coefficients.

As shown in Fig. 5, the damping of the two terms in the series of ϕ is quite good. It is clearly shown that the torsional vibrations are uncoupled to the other displacements and there is not any noticeable coupling between the vibrations of ϕ_1 and ϕ_2. As can be seen from the figure the blade is torsionally very stiff.

It is worth pointing out that the frequencies of the natural vibrations of the different modes agrees very well with calculations which are based on available formulas from the literature (this is a case of uniform blade for which such formulas exist).

In Fig. 6 the displacements distributions along the blade, for $\psi=30^\circ$, are presented. It is clear from the previous figure that in all the series the first element is the most significant one. In the case of w it is shown very clearly that the rigid body flapping (w_1) is indeed the most significant term, but there is also a noticeable elastic deflection. At later azimuthal positions, the shape of w becomes much closer to a straight line since the elastic deformations become very small compared to the rigid body flapping.

In Fig. 7 the spanwise distributions of the resultant moment components are presented (for the azimuthal location $\psi=30^\circ$). For each component, the

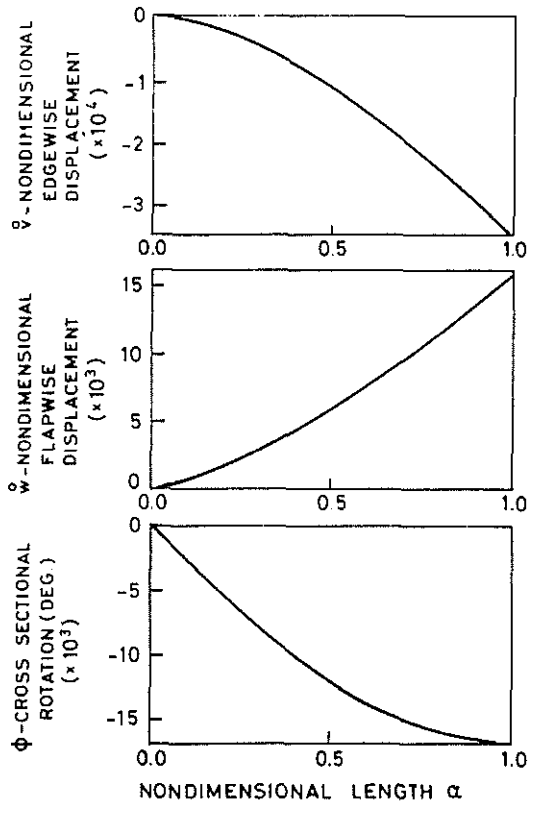

Fig. 6. Case 3.1 - spanwise distribution of the displacements (ψ=30°).

results of the differentiation method are compared with those of the integration method. Similar comparison have also been presented in [12]. In general, the agreement between these methods is very good. The largest discrepancies appear in the torsional moment, M_X, which is much smaller than the other two components. In Fig. 8 the distributions of the resultant moment components, for the azimuthal location ψ=150°, are presented. In the case of M_Y relatively large discrepancies (compared to ψ=30°) between the results of the two methods exist at the inner sections of the blade. There are also larger discrepancies in M_Z, compared to the case of ψ=30°, while the agreement in M_X is better. Similar distributions have also been obtained for many other azimuthal locations and it can be concluded that there are cases where the agreement between both methods of calculations is excellent while in other cases there are discrepancies similar to those of Fig. 8.

The distribution of P is not presented here, but it is worth pointing out that in all the cases which have been checked the agreement between P which is obtained from Eq. (24-a) and P which is obtained by integration, is excellent.

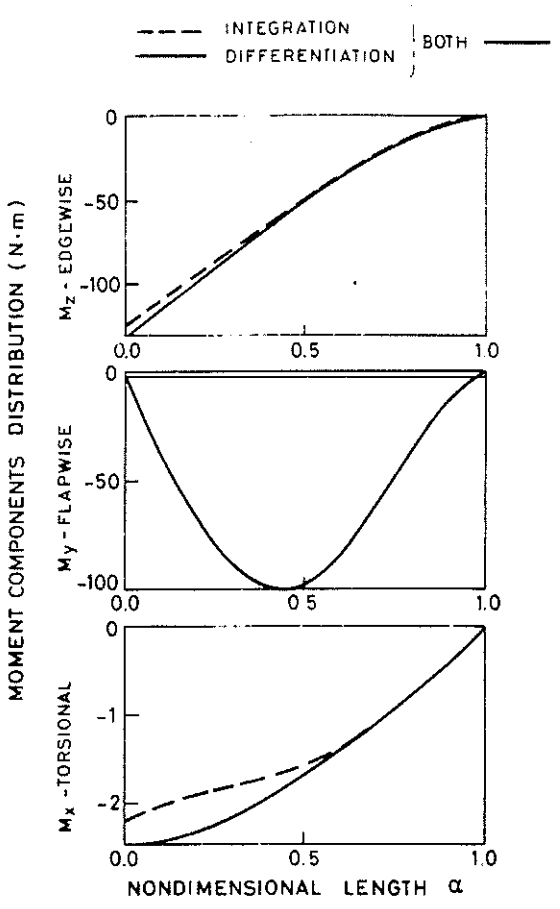

Fig. 7. Case 3.1 - spanwise distribution of the resultant moment (ψ=30°).

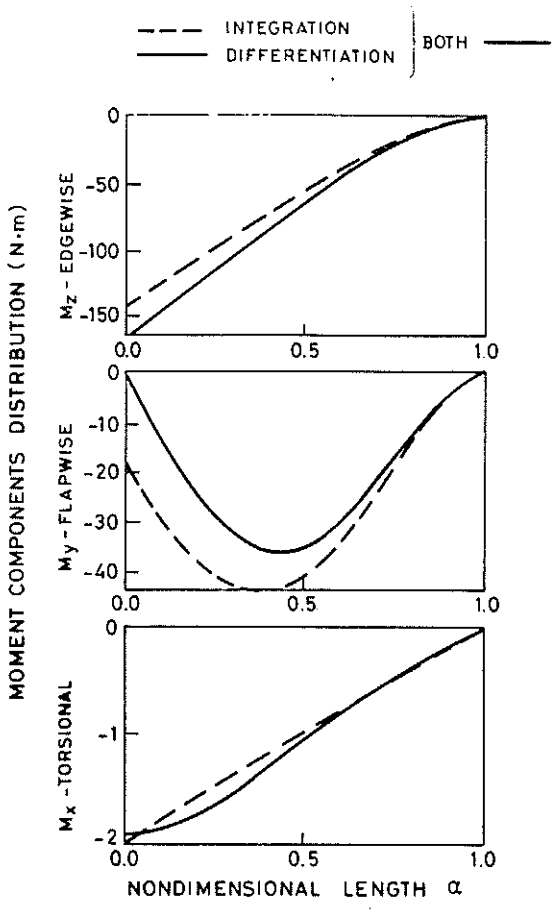

Fig. 8. Case 3.1 - spanwise distribution of the resultant moment (ψ=150°).

3.2 Flapping Hinge - Solution by Root Dynamics

This case is physically identical to the previous case and the only difference is the method of solution. Here, instead of describing the rigid body flapping by the first term in the series which describes w, this flapping is described by the angle β which is calculated by introducing root dynamics (see subsection 2.5). As indicated before, the root dynamics method does not include any assumptions concerning the magnitude of the motions at the blade root. On the other hand, the cases where the rigid body flapping is modeled as a deflection mode include different approximations which have been introduced into the structural analysis of the blade.

The different variables, as functions of time, are presented in Fig. 9. Comparison of Figs. 5 and 9 implies that β agrees perfectly well with w_1 of the previous case. FW_1 and FW_2 in the present case are identical to FW_2 and FW_3 of the previous case, respectively. Therefore, it is not

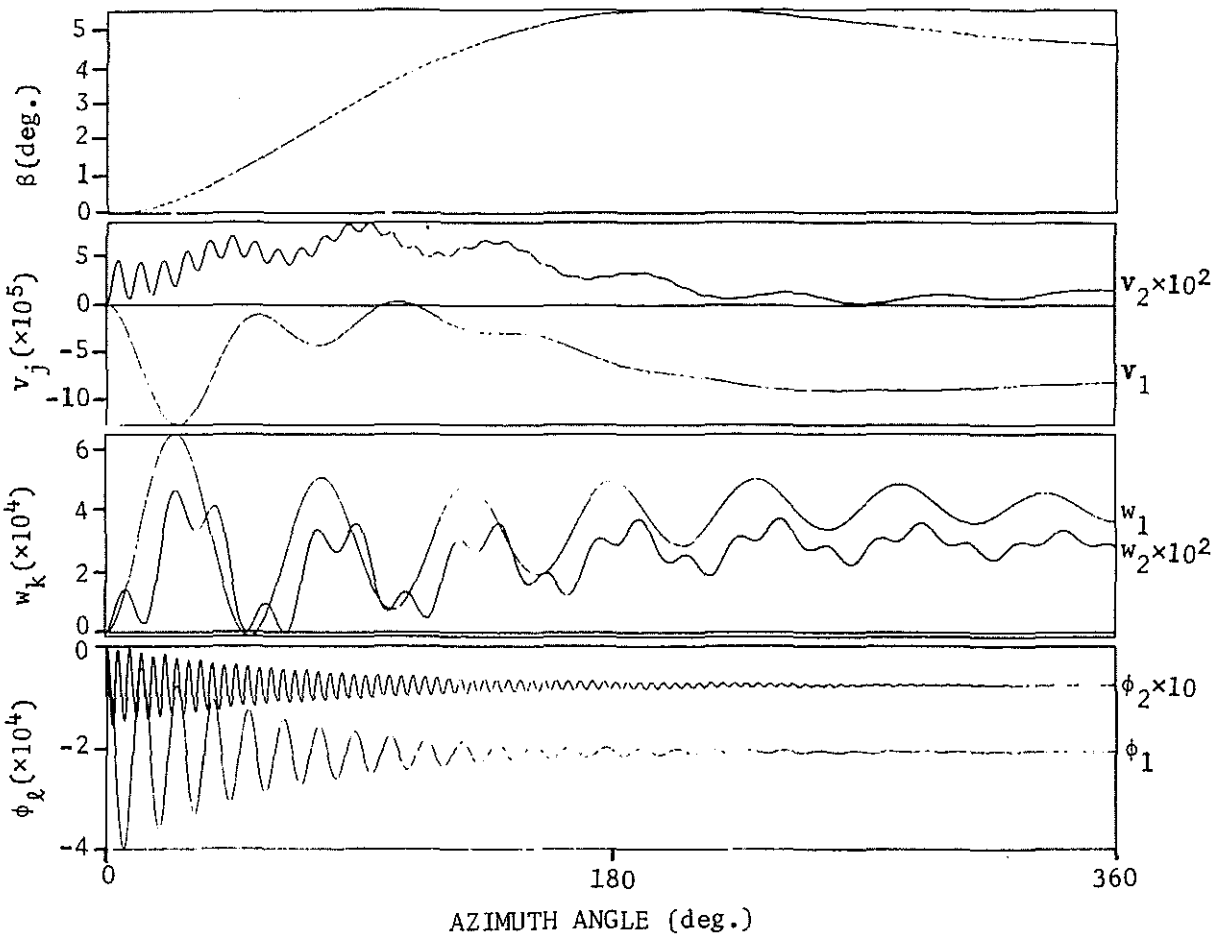

Fig. 9. Case 3.2 - time response of the coefficients.

surprising that the behavior of w_1 and w_2 in Fig. 9 is identical to the behavior of w_2 and w_3, respectively, in Fig. 5. All the other shape functions in the present subsection are identical to those of the previous one and therefore the behavior of v_2, ϕ_1 and ϕ_2 in Fig. 9 agrees very well with the behavior of the same variables in Fig. 5. The only significant difference appears in the case of v_1. While the initial response is very similar in both cases (the initial response is the region $0 \leq \psi < 130^\circ$), the lightly damped vibrations which appear after the initial response of Fig. 5, are highly damped and almost disappear in Fig. 9. It is interesting to note that unlike Fig. 5, in Fig. 9 v_1 and w_2 are in anti-phase during all the time. The explanation to the different behavior of v_1 is probably the more accurate approach of using β instead of w_1 of the previous case.

In Fig. 10 the distributions of the resultant moment components, for $\psi=150^\circ$, are presented. Unlike the same case which has been presented in Fig. 8, in Fig. 10 the agreement between the two methods of calculations is

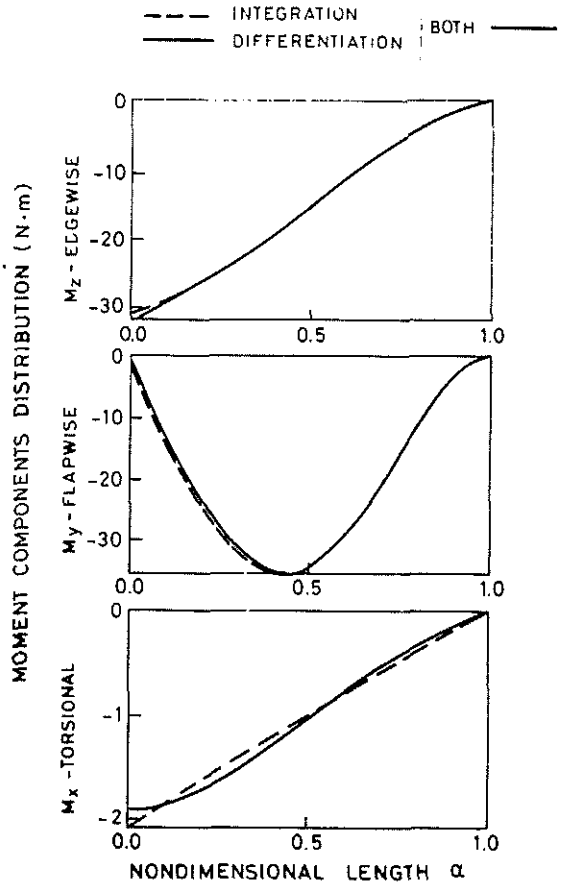

Fig. 10. Case 3.2 - spanwise distribution of the resultant moment (ψ=150°).

very good and even surprising. Such a good agreement has also been obtained in all the other azimuthal locations which has been checked and is again probably the result of using the more accurate approach of root dynamics. While numerically M_X and M_Y of Figs. 8 and 10 are very similar, M_Z is similar in shape but completely different in magnitude. This difference results from the differences in the behavior of v_1 which have been discussed previously.

3.3 Flapping Constraint

In this case (as in the previous one) root dynamics is used in order to present the rigid body rotations about the flapping hinge. The present case is identical to the previous case (subsection 3.2) except from the fact that the blade is not completely free to rotate about the flapping hinge. Instead there is a flapping restraint which is represented by a linear torsional spring having a stiffness of 6 kN m/rad. When β=0 the spring does not exert any moment on the blade root. Another minor difference between the present case and the one of subsection 3.2 is the fact that at ψ=0 (as shown in Fig. 11) v_1, v_2, w_2 and w_3 have finite values and they are not equal to zero as in the previous subsection.

In Fig. 11 the time response of the different coefficients is presented. The behavior of β is similar to its behavior as has been presented in Fig. 9. As a result of the flapping restraint, the magnitude of β is significantly smaller. In addition, since the natural frequency of the rigid body flapping has been increased, β (in Fig. 11) obtains its maximum value earlier than in Fig. 9. FW_1 is the first mode of vibration of a

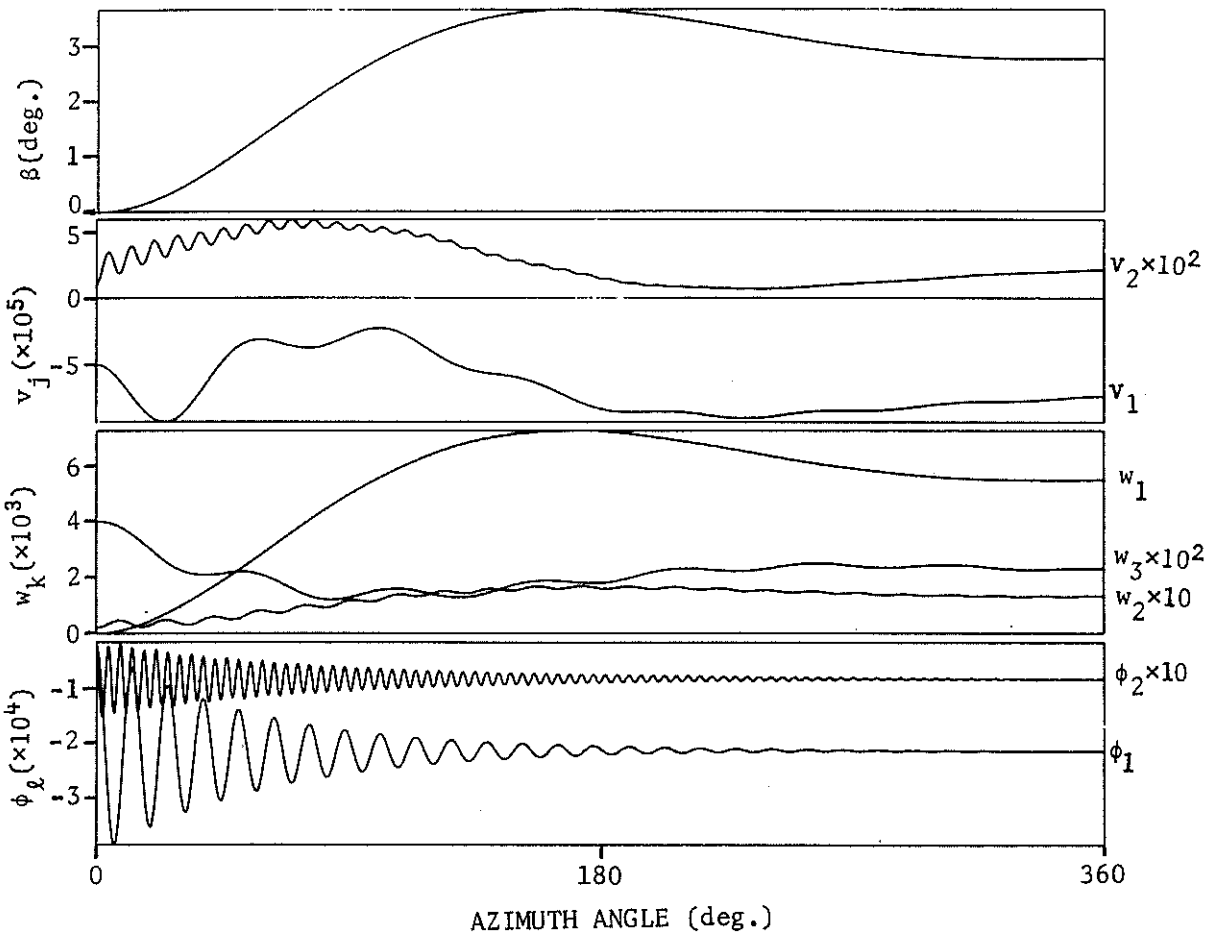

Fig. 11. Case 3.3 - time response of the coefficients.

uniform clamped/free beam. This shape function is responsible for the resultant flapping moment at the blade root which is linearily proportional to the blade flapping angle. Therefore, the behavior of w_1 follows that of β. FW_2, FW_3, FV_1, FV_2, $F\phi_1$ and $F\phi_2$ are identical to the same shape functions in the case of subsection 3.1. The behavior of w_2 and w_3 shows that if they begin (at ψ=0) from appropriate values, which are not zero, their behavior is more "calm" and the transient which was shown in Figs. 5,9, has almost disappeared. The behavior of v_1, v_2, ϕ_1 and ϕ_2 in Fig. 11 is similar to their behavior in Fig. 9.

While the distributions of M_x and M_z in the present case are similar to their distributions in the previous cases and therefore are not presented, the spanwise distribution of M_y is basically different and therefore it will be discussed in what follows. In Fig. 12 the distribution of M_y in two azimuthal locations is presented. At $\psi=12^\circ$ the flapping angle at the blade root is still very small and therefore the flapping moment there (which is proportional to this angle) is also very small and so the

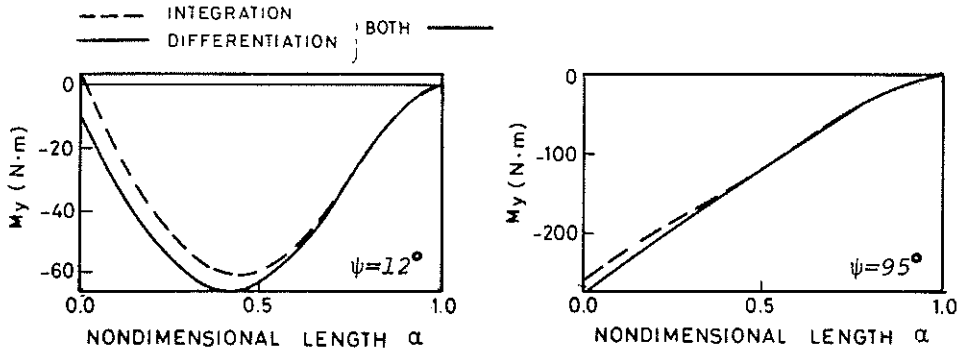

Fig. 12. Case 3.3 - spanwise distribution of the flapwise component of the resultant moment ($\psi=12^\circ$, 95°).

distribution of M_y is similar to its distribution in the previous cases. At $\psi=95^\circ$ the flapping angle has reached a significant value and therefore there is a significant flapwise moment at the blade root. This moment results in a distribution of M_y which is typical for a clamped/free blade like in the case of hingeless rotors.

4. Conclusions

A general model of blade dynamics has been described. This model is very flexible and can accommodate with any motion of the rotor, any kind of rotor (articulated, teetering, hingeless etc.) and any attachment of the blade to the hub. In addition the model can deal with curved blades having any spanwise distribution of the structural, geometric, mass and aerodynamic properties. Only very few assumptions have been adopted and therefore the model is applicable to almost all the practical cases, without any restrictions.

Special attention has been devoted to the root dynamics. The root dynamics analysis is very accurate and there is not any restriction concerning the magnitude of the displacements or rotations at the blade root. Such an approach is very important if one is interested in avoiding unpredictable errors.

Galerkin method, as similarily pointed out in other researches in the past, is a very efficient way of solving problems of blades' dynamics. The

convergence of this method is relatively fast and the number of unknowns associated with this method is relatively small compared with other methods which are used for the same kind of problems.

The resultant forces and moments along the blade can be calculated by using two methods. The first method is based on differentiation of the displacements while the second method includes integration of the loads along the blade. In the present examples of relatively stiff blades, the agreement between the results of the two methods ran between excellent and good agreement. From numerical analysis theory it is expected that the results of the integration will be more accurate. Anyway, comparison of both methods is always a good mean of checking the results.

The implicit Adam's method is a very accurate, convenient and relatively efficient method for the integration of the equations of motion.

The main purpose of this paper was to present the possibility of obtaining a relatively accurate model of the blade dynamics which is yet very general and is able to solve many different practical cases of blades under different modes of operation. This model will be used in the future in order to investigate the dynamics of different blades at different operation conditions. In the future the possibility of combining this shophisticated dynamic model with much more complicated aerodynamic models (compared to the aerodynamic model of the present paper) will also be investigated.

Acknowledgement

The authors would like to thank Mrs. Goodman-Pinto for typing the manuscript and Mrs. E. Nitzan for preparing part of the figures.

List of References

1) P.J. Arcidiacono: Prediction of Rotor Instability at High Forward Speeds, Volume I - Steady Flight Differential Equations of Motion for a Flexible Helicopter Blade with Chordwise Mass Unbalance. Prepared by United Aircraft Corporation, Sikorsky Aircraft Division, Stratford, Connecticut, USAAVLABS Technical Report 68-18a, February 1969.

2) R.A. Piziali: An Investigation on the Structural Dynamics of Helicopter Rotors. Cornell Aeronautical Laboratory, Inc., Buffalo, New York, USAAVLABS Technical Report 70-24, April 1970.

3) W.D. Anderson: REXOR Rotorcraft Simulation Model, Volume I - Engineering Documentation. Lockheed California Co., USAAMRDL-TR-76-28A, July 1976.

4) J.R. Van Gaasbeek, T.T. McLarty and S.G. Sadler: Rotorcraft Flight Simulation, Computer Program C81, Volume I - Engineer's Manual. Bell Helicopter Texteron, USARTL-TR-77-54A, October 1979.

5) W. Johnson: Development of a Comprehensive Analysis for Rotorcraft - I. Rotor Model and Wake Analysis. Vertica, Vol. 5, 1981, pp. 99-129.

6) W. Johnson: Development of a Comprehensive Analysis for Rotorcraft - II Aircraft Model, Solution Procedure and Applications. Vertica, Vol. 5, 1981, pp. 185-216.

7) A. Rosen and O. Rand: A General Model of the Dynamics of Moving and Rotating Curved Rods. TAE Report No. 514, August 1983.

8) C.W. Gear: Numerical Initial Value Problems in Ordinary Differential Equations. Prentice-Hall, Englewood Cliffs, New Jersey, 1971.

9) R.L. Bisplinghoff, H. Ashley and R.L. Halfman: Aeroelasticity. Addison-Wesley Publishing Co. Inc., 1957, pp. 272.

10) D. Young and R.P. Felgar, Jr.: Tables of Characteristic Functions Representing Normal Modes of Vibration of Beam. The University of Texas Publications, No. 4913, July 1949.

11) A.R.S. Bramwell: Helicopter Dynamics. John Wiley and Sons, New York, 1976.

12) R.L. Bielawa: Blade Stress Calculations - Mode Deflection vs. Force Integration. J. Amer. Hel. Soc., Vol. 24, No. 3, July 1978, pp. 10-16.

Appendix - The Properties of the Blade

Length (L)	1.52(m)
Chord (c)	0.122(m)
Flapwise bending stiffness (EI_{zz})	11,500(N m^2)
Edgewise bending stiffness (EI_{yy})	258,000(N m^2)
Compound bending stiffness (EI_{yz})	0
Torsional stiffness (GJ)	8,000(N m^2)
Components of the cross sectional mass moments of inertia MI_{zz}	0.1 10^{-4}(kg m)
MI_{yy}	0.46 10^{-3}(kg m)
MI_{yz}	0.63 10^{-4}(kg m)
Mass per unit length (m)	0.535(kg/m)
Lift coefficient curve slope	5.9(1/rad)
Drag coefficient properties (see Eq. 30)	δ_0 = 0.01
	δ_1 = 0
	δ_2 = 0.015
Aerodynamic moment coefficient (c_{MAC})	0
Rotational Speed (Ω)	150 (rad/sec)
Air density (ρ_A)	1.23(kg/m^3)

The cross sectional elastic center, aerodynamic center and center of mass coincide.